

Article

PM_{2.5} Source Apportionment and Implications for Particle Hygroscopicity at an Urban Background Site in Athens, Greece

Evangelia Diapouli *, Prodromos Fetfatzis , Pavlos Panteliadis, Christina Spitieri, Maria I. Gini , Stefanos Papagiannis, Vasiliki Vasilatou and Konstantinos Eleftheriadis 

Institute of Nuclear & Radiological Science & Technology, Energy & Safety, National Centre of Scientific Research "Demokritos", 15341 Athens, Greece

* Correspondence: ldiapouli@ipta.demokritos.gr

Abstract: Aerosol hygroscopicity is a key aerosol property, influencing a number of other physical properties, and the impacts of PM pollution on the environment, climate change, and health. The present work aims to provide insight into the contribution of major PM sources to aerosol hygroscopicity, focusing on an urban background site, with a significant impact from both primary and secondary sources. The EPA PMF 5.0 model was applied to PM_{2.5} chemical composition and hygroscopicity data collected from August 2016 to July 2017 in Athens, Greece. Source apportionment analysis resulted in six major sources, including four anthropogenic sources (vehicular exhaust and non-exhaust, heavy oil combustion, and a mixed source of secondary aerosol formation and biomass burning) and two natural sources (mineral dust and aged sea salt). The mixed source was found to be the main contributor to PM_{2.5} levels (44%), followed by heavy oil combustion (26%) and vehicular traffic exhaust and non-exhaust emissions (15%). The aerosol hygroscopic growth factor (GF) was found to be mainly associated with the mixed source (by 36%) and heavy oil combustion (by 24%) and, to a lesser extent, with vehicle exhaust (by 19%), aged sea salt (by 14%), and vehicle non-exhaust (by 6%).

Keywords: PM_{2.5}; hygroscopicity; source apportionment; positive matrix factorization; urban background



Citation: Diapouli, E.; Fetfatzis, P.; Panteliadis, P.; Spitieri, C.; Gini, M.I.; Papagiannis, S.; Vasilatou, V.; Eleftheriadis, K. PM_{2.5} Source Apportionment and Implications for Particle Hygroscopicity at an Urban Background Site in Athens, Greece. *Atmosphere* **2022**, *13*, 1685. <https://doi.org/10.3390/atmos13101685>

Academic Editor: László Bencs

Received: 22 August 2022

Accepted: 11 October 2022

Published: 14 October 2022

Publisher's Note: MDPI stays neutral with regard to jurisdictional claims in published maps and institutional affiliations.



Copyright: © 2022 by the authors. Licensee MDPI, Basel, Switzerland. This article is an open access article distributed under the terms and conditions of the Creative Commons Attribution (CC BY) license (<https://creativecommons.org/licenses/by/4.0/>).

1. Introduction

Suspended particulate matter (PM) remains an atmospheric pollutant of great concern, especially in urban centres, where anthropogenic emission sources are concentrated and a large share of the global population resides. Particulate pollution contributes to climate change and visibility degradation; impacts the atmospheric chemical processes, affecting the concentration of gaseous pollutants; and displays documented adverse effects on human health [1,2]. In order to fully understand the different impacts of particulate pollution, a comprehensive characterization of the atmospheric aerosol is needed, including its physical and chemical properties.

Aerosol hygroscopicity, i.e., the ability of particles to absorb water in response to increasing relative humidity, is a key aerosol property, influencing a number of other physical properties, and the impacts of PM pollution on the environment, climate, and health. The water content of particles affects their size and surface area, as well as the total aerosol mass, acidity, chemical reactivity, and atmospheric lifetime [3,4]. Particle hygroscopicity also affects the aerosol optical properties, with significant implications for visibility and radiative forcing [5–7]. In addition, hygroscopic growth is directly associated with aerosol cloud droplet activation properties, which impact climate change [8]. Hygroscopicity is also strongly associated with particle health impacts. Hygroscopic particles grow significantly in the near supersaturated environment of the respiratory tract; this may substantially alter

particle deposition (both with respect to lung deposition probability and place of deposition), as well as the metabolic pathway after deposition, in comparison with non-soluble particles [9,10].

The atmospheric aerosol ability to absorb water depends on its chemical composition and mixing state [11,12]. Fossil fuel combustion processes usually emit hydrophobic or slightly hygroscopic particles [9], while biomass burning emissions may also contain hygroscopic particles [13]. Secondary inorganic aerosols (e.g., ammonium sulfate and nitrate) are hydrophilic. With respect to primary natural particles, sea salt particles are hygroscopic, while soil dust particles are normally insoluble [4]. Among the different aerosol species, the less characterized in terms of hygroscopic growth is organic aerosol, owing to the wide range of organic compounds found in the atmosphere. It is generally expected that aged and more oxidized organic aerosol will be more hygroscopic [14]; nevertheless, it has been shown that hygroscopic growth is not always correlated with the O=C ratio, demonstrating that other factors also play an important role (such as the different functional groups, carbon chain length, and so on) [15]. These uncertainties related to organic aerosol hygroscopic properties hamper a better understanding of the role of primary and secondary organic matter in the atmospheric environment and climate [16].

Several studies have attempted to link aerosol hygroscopic behavior with chemical composition [15,17–21] or to characterize hygroscopic properties of various aerosol types, based on air mass back trajectories or specific pollution episodes [22–24]. In addition, the hygroscopic properties of particles emitted by typical combustion processes, such as diesel vehicle exhaust [25,26] and biomass burning emissions [27–30], have been assessed. Nevertheless, while it has been acknowledged that hygroscopicity is highly dependent on both aerosol emission sources and atmospheric transformations, the hygroscopic properties of the various sources in receptor sites, where freshly emitted and aged aerosol are mixed, have been scarcely explored. To the best of our knowledge, only two very recent studies have attempted to evaluate the hygroscopicity of major PM sources identified by receptor modelling. Li et al. performed a source apportionment study combining PM_{2.5} chemical composition data with hygroscopicity measurements from a 3-month period, during 2019–2020, in an urban site of Guangzhou, China [31]. Vu et al. applied receptor modelling for source apportionment of sub-micrometer particles, using particle number size distribution data together with hygroscopicity data, collected at an urban background site in London, United Kingdom, during two 2-month campaigns in 2012, covering cold and warm season [32]. Both studies confirmed the good potential of PMF in characterizing the hygroscopic properties of particles originating from different primary and secondary sources. The most hydrophilic sources were related to secondary inorganic aerosol and mixed secondary organic and inorganic aerosol; the less-hygroscopic particles were associated with primary combustion emissions and soil dust [31,32].

The present work aims to provide further insight into the contribution of PM sources to aerosol hygroscopicity, focusing on an urban background site, with a significant impact from both primary and secondary sources. A year-long measurement campaign was performed during 2016–2017 at the Demokritos (DEM) urban background station, in Athens, Greece, including PM_{2.5} chemical speciation and hygroscopicity measurements. Limited hygroscopicity data are available for Southern Europe, and Greece in particular. Hygroscopicity measurements were performed at a regional background site in the island of Crete [22] and a background site in the island of Lemnos [33]. Data on urban aerosol hygroscopicity in Greece have been reported only for Athens, during a short campaign (11–26 June 2003) at a suburban background site, and at DEM station for the year-long campaign of 2016–2017 [34,35]. In the present work, these latter data were used together with concurrent PM_{2.5} chemical composition data in order to apply receptor modelling for PM and hygroscopicity source apportionment. Source apportionment analysis resulted in six major sources, including four anthropogenic sources (vehicular exhaust and non-exhaust, heavy oil combustion, and a mixed source of secondary aerosol formation and biomass burning) and two natural sources (mineral dust and aged sea salt). The aerosol

hygroscopic growth factor (GF) was found mainly associated with the mixed source (by 36%) and heavy oil combustion (by 24%) and, to a lesser extent, with vehicle exhaust (by 19%), aged sea salt (by 14%), and vehicle non-exhaust (by 6%).

2. Materials and Methods

2.1. PM Sampling and Analysis

A year-long measurement campaign was conducted from August 2016 to July 2017 at the Demokritos (DEM) urban background station, in Athens, Greece (37.995° N 23.816° E, at 270 m above sea level (a.s.l.)), a member of GAW and part of the ACTRIS and PANACEA infrastructures (Figure 1). The station is away from direct emissions; the site is partially influenced by the urban area (i.e., under most atmospheric conditions) and partially by the incoming regional aerosol (i.e., under northern or southern winds), and can be considered as typical for a suburban Mediterranean atmospheric environment [36]. The climate is characterized by hot dry summers and wet mild winters. During the measurement campaign, the ambient temperature was measured to be equal to $10.9 \pm 4.4^{\circ}$ C in the cold period (15 October 2016–14 April 2017) and $23.5 \pm 4.7^{\circ}$ C in the warm period (1 August–14 October 2016 and 15 April–31 July 2017).

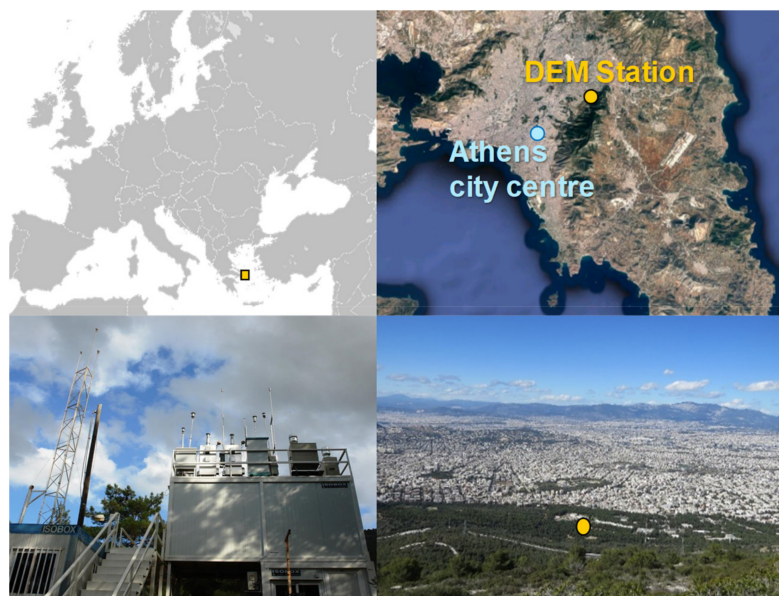


Figure 1. The Demokritos (DEM) urban background station in Ag. Paraskevi, Athens, Greece (37.995° N 23.816° E, at 270 m above sea level (a.s.l.)).

In this research, 24 h $PM_{2.5}$ samples were collected by a low-volume reference sampler (Sequential 47/50-CD, Sven Leckel GmbH, Berlin, Germany) at a flow rate of $2.3 \text{ m}^3/\text{h}$ on Teflon filters and were analyzed gravimetrically for the determination of PM mass concentrations, according to EN12341. The samples were also analyzed by X-ray fluorescence (XRF) with the use of an energy dispersive x-ray fluorescence spectrometer (ED-XRF) laboratory instrument (Epsilon 5, PANalytical, Malvern, UK). The following major and trace elements were determined: Na, Mg, Al, Si, S, Cl, K, Ca, Ti, V, Cr, Mn, Fe, Ni, Cu, Zn, Br, Ba, and Pb. Detection limits ranged from $0.2 \text{ ng}/\text{m}^3$ (for Cr) to $16.2 \text{ ng}/\text{m}^3$ (for Ba). Details on the method may be found in Manousakas et al. [37].

Near-real time elemental (EC) and organic carbon (OC) concentrations in $PM_{2.5}$ were recorded on a 3 h basis, using the thermo-optical transmittance (TOT) method, using a semi-continuous OC-EC field analyzer (Model-4, Sunset Laboratory, Inc., Tigard, OR, U.S.A.), equipped with an in-line parallel carbon denuder for the removal of organic gases. The EUSAAR2 protocol was employed for analysis. The output of the analyzer includes the different OC fractions (OC1 to OC4) corresponding to the four temperature steps of the

EUSAAR2 protocol (at 200 °C, 300 °C, 450 °C, and 650 °C); the pyrolytic organic carbon (POC), formed through pyrolysis during the thermal volatilization of OC; and the elemental carbon (EC). The OC fractions provide insight into the volatility of the different organic compounds, with OC1 representing the more volatile OC fractions and OC4 and POC the less volatile fractions [38]. Details on the method may be found in Panteliadis et al. [39].

In addition, a custom-built humidified tandem differential mobility analyzer (HTDMA) was used to measure the hygroscopic growth factor distributions of ambient aerosol particles with selected dry diameters (D_0) of 30 nm, 50 nm, 80 nm, and 250 nm (at a relative humidity of $30 \pm 3\%$), exposed to a relative humidity (RH) of $90 \pm 2\%$. Owing to water uptake, the diameter of the humidified particles ($D(\text{RH})$) increased and the ratio between the humidified ($D(\text{RH})$) and dry particle diameter (D_0) was defined as the growth factor (GF):

$$\text{GF} = \frac{D(\text{RH})}{D_0} \quad (1)$$

The particle concentration at the HTDMA outlet as a function of the growth factor is referred to as the measurement distribution function (MDF). An inversion algorithm was applied to the measured MDF to retrieve the actual growth factor probability density functions (GF-PDFs), which describe the probability that a particle with a defined dry size exhibits a certain GF at the specified relative humidity. Details on the HTDMA system and the inversion algorithm applied may be found in Spitieri et al. [35].

2.2. Source Apportionment by Positive Matrix Factorization

Source apportionment was performed by means of receptor modeling, specifically the positive matrix factorization (PMF) model. PMF is a widely used receptor model, which allows for the identification of the major PM sources, based on their chemical profiles, as well as the quantification of their contribution to the measured PM concentration levels [40]. The model is based on the following mass balance equation:

$$c_{ij} = \sum_{k=1}^p g_{ik} \cdot f_{kj} + e_{ij} \quad (2)$$

where c_{ij} is the concentration of chemical element j measured in sample i , p is the number of factors (sources) that contribute to the measured concentrations, g_{ik} is the contribution of source k to sample i , f_{kj} is the concentration of the chemical element j in source k , and e_{ij} is the residual (the difference between the measured value and the value fitted by the model) for chemical element j in sample i .

The model solves Equation (2) by minimizing the sum of squared residuals, as shown in Equation (3) below:

$$Q = \sum_{i=1}^n \sum_{j=1}^m \left(\frac{c_{ij} - \sum_{k=1}^p g_{ik} \cdot f_{kj}}{u_{ij}} \right)^2 = \sum_{i=1}^n \sum_{j=1}^m \left(\frac{e_{ij}}{u_{ij}} \right)^2 \quad (3)$$

where u_{ij} is the uncertainty of the concentration value c_{ij} . PMF produces two matrices (F—factor profiles and G—factor contributions) under the constraint of non-negativity for matrix F and non-significant negativity for matrix G.

In the present work, the EPA PMF 5.0 model was applied to the $\text{PM}_{2.5}$ chemical composition database in order to quantify the contribution of the different sources to the observed $\text{PM}_{2.5}$ concentration levels; at a second stage, the model was applied to the combined chemical composition and hygroscopicity data in order to explore the hygroscopicity of the major PM sources identified. The hygroscopic growth factor (GF) of particles with dry diameters (D_0) of 250 nm was used in this analysis. This particle size fraction corresponds to the accumulation mode and may be thus considered representative of the $\text{PM}_{2.5}$ hygroscopic properties. The OC/EC and hygroscopicity data were averaged to match the 24 h $\text{PM}_{2.5}$ concentration data. Overall, the database comprised 265 sampling days and 26 input variables, including 24 variables defined as “strong”: EC, OC1, OC2, OC3, OC4, Na, Mg,

Al, Si, S, Cl, K, Ca, Ti, V, Cr, Mn, Fe, Ni, Cu, Br, Ba, Pb, and GF, and two variables defined as “weak”: POC and Zn. PM_{2.5} mass concentration was included as the total variable in the initial analysis (without GF as an input variable). The expanded uncertainty (including sampling and analytical uncertainties) was calculated for all input data and ranged from 10 to 40% for values above the detection limit. For values below the detection limit, the uncertainty was set equal to 5/6 of the detection limit. Missing values in the datasets were substituted by the median of the respective time series, calculated separately for each season. The uncertainty for these values was set equal to four times the concentration value. An extra modeling uncertainty of 5% was added to account for modeling errors. The model was run for different numbers of sources, ranging from 4 to 10 sources. The best solution was identified through the use of key performance indicators, including the lowest *Q* values, distribution of scaled residuals, and fit of measured PM concentrations, as well as by assessing the physical meaning of the obtained source profiles and contributions. The final solutions were based on 100 runs, while the uncertainty of the solutions was assessed by implementing the bootstrapping and displacement error estimation tools provided by EPA PMF 5.0 [41].

3. Results

3.1. PM_{2.5} Chemical Composition and Hygroscopicity

The mean annual PM_{2.5} concentration was measured equal to $10.5 \pm 4.0 \mu\text{g}/\text{m}^3$, below the EU annual limit value of $25 \mu\text{g}/\text{m}^3$. Carbonaceous particles accounted for a large fraction of the PM mass. OC and EC were measured on average equal to $2.1 \pm 1.0 \mu\text{g}/\text{m}^3$ and $0.4 \pm 0.3 \mu\text{g}/\text{m}^3$, respectively. The average OC-to-EC concentration ratio (OC/EC) was calculated equal to 5.4 ± 2.5 , indicative of the urban background character of the site [42]. Assuming an organic mass (OM) to organic carbon (OC) ratio of 1.7 [43], carbonaceous aerosol (OM + EC) was calculated to comprise on average $42 \pm 22\%$ of the total PM_{2.5} mass. The most abundant species, following carbonaceous matter, was S, with an average concentration of $0.5 \pm 0.5 \mu\text{g}/\text{m}^3$.

The seasonal variability of all measured concentrations is provided in Table 1. PM_{2.5}, as well as many PM components, displayed a significant difference (at $p = 0.01$) between cold and warm period concentrations. Carbonaceous aerosol was higher during the cold period, pointing towards an additional carbon source, related to residential heating. The OC/EC ratio, however, did not display a significant difference between heating (cold) and non-heating (warm) periods, suggesting a limited contribution from residential wood burning. The concentrations of S and crustal components (Al, Si, K, Ca, Ti, and Fe) were higher during the warm period. Sulphate, which is the main form of S in the atmosphere, is formed photochemically, and thus is expected to be present in higher concentrations during the warm months, when solar radiation is more intense. The high levels of crustal components during this season are also expected as a result of the dry conditions that promote soil dust resuspension.

Table 1. Seasonal variability of PM_{2.5} and measured chemical components’ concentrations. PM_{2.5} concentrations are provided in $\mu\text{g}/\text{m}^3$ and all components’ concentrations in ng/m^3 . Species that display statistically significant difference in concentrations between warm and cold periods (at $p = 0.01$) are marked in bold.

	Cold Period			Warm Period		
	Median	Range		Median	Range	
PM _{2.5}	9.4	2.9	18.8	10.5	4.8	24.7
OC	2280	436	6582	1762	737	4067
EC	469	99	1725	327	BDL ¹	1096
OC/EC	4.5	2.0	12.5	4.6	1.9	17.0

Table 1. Cont.

	Cold Period			Warm Period		
	Median	Range		Median	Range	
Na	36.4	BDL	594	31.1	BDL	369
Mg	3.6	BDL	319	2.2	BDL	252
Al	4.8	BDL	517	34.7	BDL	567
Si	5.4	BDL	1295	76.1	BDL	1238
S	109	12.7	1595	526	23.2	1812
Cl	1.2	BDL	638	0.8	BDL	53.5
K	16.4	3.3	342	78.5	1.6	345
Ca	11.8	0.7	431	82.5	2.6	437
Ti	0.8	BDL	40.5	3.3	BDL	39.2
V	0.5	BDL	6.9	0.6	BDL	7.2
Cr	0.4	BDL	4.1	0.3	BDL	3.5
Mn	1.0	BDL	5.4	1.0	BDL	7.2
Fe	10.5	1.0	369	63.3	3.0	361
Ni	0.8	BDL	12.4	0.6	BDL	11.2
Cu	0.6	BDL	15.8	0.6	BDL	13.4
Zn	2.8	BDL	36.0	3.5	BDL	49.5
Br	1.1	BDL	7.6	1.1	BDL	6.3
Ba	13.5	BDL	13.5	8.1	BDL	18.4
Pb	1.9	BDL	17.6	1.4	BDL	18.4

¹ Value below the detection limit.

The median value of the hygroscopic growth factor, at 90% relative humidity, for particles with a dry diameter at 250 nm, was measured equal to 1.21 ± 0.07 . The cold and warm period values were 1.22 ± 0.06 and 1.18 ± 0.07 , respectively.

3.2. PM_{2.5} and Hygroscopicity Source Apportionment

The assessment of the different PMF solutions, in terms of the goodness of fit of input data and physical meaning of the obtained factors, led to the identification of the six-factor solution as the one that best described the input data, for both cases of model application (including and without the hygroscopicity as an input parameter). The source profiles obtained for the full dataset (including the hygroscopic growth factor) are presented in Figure 2. The apportionment of different species to each factor/source is presented in Figure 3. The initial PMF analysis, without hygroscopicity data, provided almost identical source profiles to the ones displayed in Figure 3, in terms of the relative mass contribution of the different chemical components to the profiles. The six major PM_{2.5} sources identified were as follows: vehicle exhaust, vehicle non-exhaust, heavy oil combustion, mixed source related to secondary aerosol formation and biomass burning, mineral dust, and aged sea salt.

The vehicle exhaust profile accounted for most of the carbonaceous species' mass (60% of EC and 75–86% of OC1–OC3 fractions). OC1–OC3 have been associated with combustion sources, including traffic, as emissions from these sources are rich in semi-volatile organic compounds [44]. The vehicle exhaust profile displayed high loadings of EC and OC1–OC4, while POC's contribution was negligible, in agreement with diesel and gasoline vehicle emission profiles reported in the literature [45,46]. The OC/EC ratio in the profile was calculated equal to 4.6, which suggests a mixture of fresh and aged exhaust emissions, in agreement with the urban background character of the site. Vehicle exhaust emissions contributed 16% ($1.5 \mu\text{g}/\text{m}^3$) during the cold period and 10% ($1.1 \mu\text{g}/\text{m}^3$) during the warm period.

The vehicle non-exhaust profile accounted for most of Cu (88%) and Pb (50%) mass. Cu and Pb are emitted during brake wear, while Pb has been also linked to asphalt wear [47]. Non-exhaust emissions' contribution to PM_{2.5} was low (2% during the cold period and 3% during the warm period), as expected, as they are related to coarse rather than fine particles.

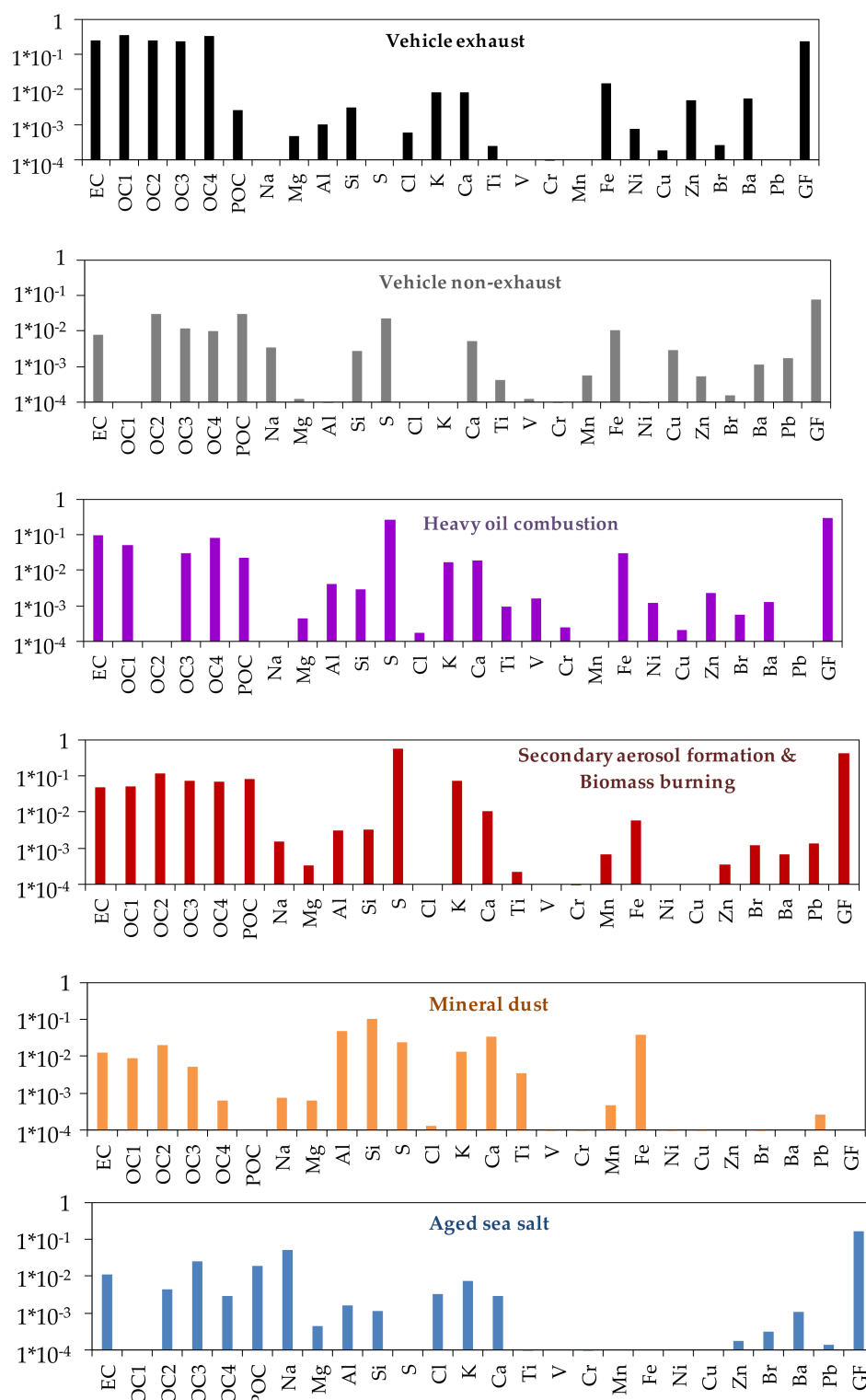


Figure 2. PM_{2.5} source profiles identified by applying PMF to the combined chemical composition and hygroscopicity data set. Chemical components’ values relate to relative mass, while GF values relate to the amount apportioned to each source by the model.

The heavy oil combustion profile was identified by V and Ni. Most of V mass (89%) and a large fraction of Ni mass (58%) were associated with this source. The profile displayed high loadings of carbonaceous species and S, as well as Fe, Ca, and K, in accordance with heavy oil combustion profiles found in the literature [48,49]. Heavy oil combustion emissions were associated with less volatile OC fractions in comparison with vehicle

exhaust [45]. This source contributed 23% ($2.2 \mu\text{g}/\text{m}^3$) during the cold period and 29% ($3.4 \mu\text{g}/\text{m}^3$) during the warm period.

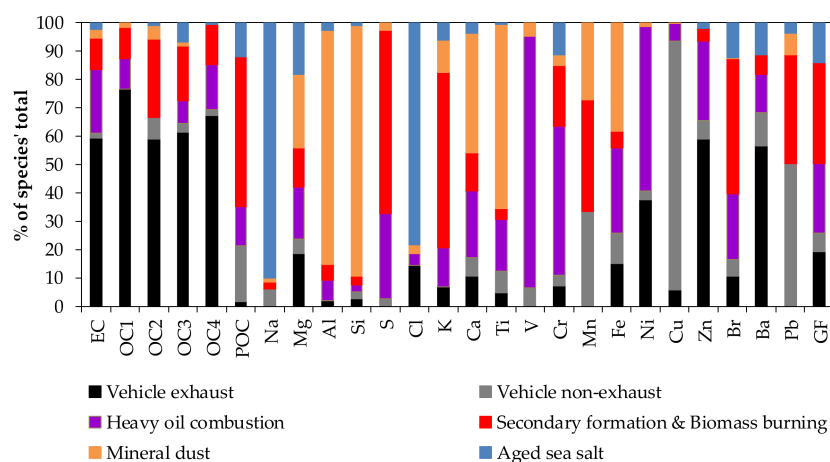


Figure 3. Relative amount of species (%) apportioned to each factor/source, obtained by applying PMF to the combined chemical composition and hygroscopicity dataset.

The fourth source identified was a mixed source of secondary aerosol formation and biomass burning. The source profile was characterized by high loadings of S and OC and accounted for 65% of total S mass, 53% of POC mass, and 62% of K mass. POC has been linked to both secondary organic aerosol formation and biomass burning emissions [44,50]; on the other hand, the biomass burning profiles reported by Liu et al. [51] demonstrate large amounts of OC1–OC4 fractions. The lack of key secondary ionic species (i.e., nitrate and ammonium) in the PM_{2.5} chemical speciation database did not allow for the identification of a separate source related to secondary aerosol formation. The mixed secondary aerosol formation and biomass burning source did not display significant seasonal variability (Figure S1, Supplementary Materials), contributing 46% to total PM_{2.5} concentrations ($4.5 \mu\text{g}/\text{m}^3$) during the cold period and 41% ($4.7 \mu\text{g}/\text{m}^3$) during the warm period.

The mineral dust profile was identified by the high loadings of crustal elements (Al, Si, K, Ca, Ti, and Fe). This profile accounted for more than 80% of the total mass of Al and Si and 65% of Ti. Mineral dust contributed 3% ($0.3 \mu\text{g}/\text{m}^3$) during the cold period and 8% ($0.9 \mu\text{g}/\text{m}^3$) during the warm period.

The aged sea salt profile was identified by the high loading of Na, while it accounted for most of Na and Cl total mass (90% and 79%, respectively). The Cl/Na mass ratio in the profile was much lower than the ratio reported for seawater, suggesting Cl depletion due to transformation of fresh sea salt aerosol through mixing with urban gaseous emissions. Aged sea salt profiles, containing high loadings of nitrate, have been previously reported for the monitoring site [43,52]. Aged sea salt contributed 5% ($0.4 \mu\text{g}/\text{m}^3$) during the cold period and 2% ($0.2 \mu\text{g}/\text{m}^3$) during the warm period.

According to PMF analysis, the aerosol hygroscopic growth factor (GF) was mainly associated with the mixed source of secondary aerosol formation and biomass burning (36%) and heavy oil combustion (24%). To a lesser extent, GF was also associated with vehicle exhaust (19%), aged sea salt (14%), and vehicle non-exhaust (6%). Mineral dust was found to be hydrophobic.

PMF analysis performed only on the chemical composition database, including PM_{2.5} as a total variable, allowed for the quantification of source contributions. The average source contributions over the whole year are presented in Figure 4. The mixed source related to secondary aerosol formation and biomass burning was found to be the main contributor to PM_{2.5} levels (44%), followed by heavy oil combustion (26%) and vehicular traffic exhaust and non-exhaust emissions (15%). Contributions from the two natural

sources (mineral dust and aged sea salt) were much lower, owing to the coarse nature of these particles.

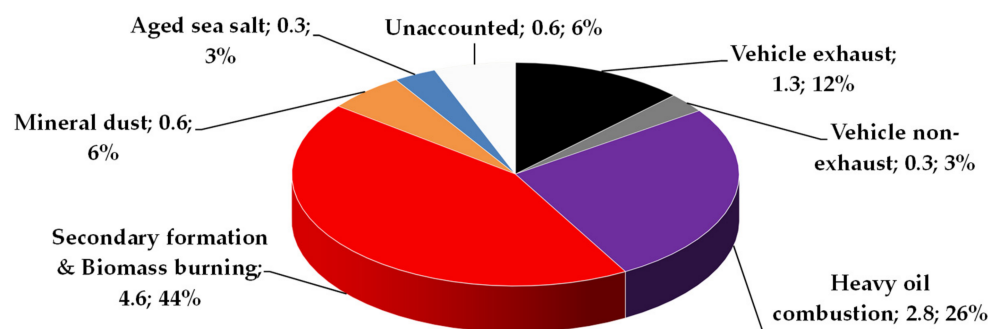


Figure 4. Average contribution (in $\mu\text{g}/\text{m}^3$ and as % of total $\text{PM}_{2.5}$ concentration) of the different sources obtained by PMF to the $\text{PM}_{2.5}$ concentration levels measured during August 2016–July 2017.

4. Discussion

The measured concentration levels of $\text{PM}_{2.5}$ and chemical constituents were generally in agreement with previous studies [43,52,53]. Over the last decade, $\text{PM}_{2.5}$ concentrations at the site were relatively low in comparison with the EU annual limit value of $25 \mu\text{g}/\text{m}^3$. Nevertheless, the levels are higher than the WHO guidelines, which recommend an annual limit value of $5 \mu\text{g}/\text{m}^3$ and a 24 h limit value of $15 \mu\text{g}/\text{m}^3$. Carbonaceous aerosol comprised a significant fraction of total $\text{PM}_{2.5}$, but a modest decrease in the total carbon (TC) concentrations was observed, with TC accounting for 24% of $\text{PM}_{2.5}$, in comparison with 27–30% during 2011–2013. This decrease was related to OC rather than EC, leading to a significant reduction in the observed OC/EC ratio (5.4 on average in this study, as opposed to 7.6–10.5 in previous years). K concentration levels were also lower in this study and the warm period levels were higher than those observed during the cold period. These results suggest that residential biomass burning was not so prominent during 2016–2017, in comparison with previous years.

The $\text{PM}_{2.5}$ chemical composition data collected during a full year (August 2016–July 2017) were combined with concurrent hygroscopicity data in order to apply PMF for source apportionment. Source apportionment of $\text{PM}_{2.5}$ concentrations resulted in six major emission sources, including four anthropogenic sources (vehicular exhaust and non-exhaust, heavy oil combustion, and a mixed source of secondary aerosol formation and biomass burning) and two natural sources (mineral dust and aged sea salt). The contribution of the natural sources to the observed $\text{PM}_{2.5}$ levels was limited (less than 10%); fine particles are known to originate mainly from anthropogenic sources.

The contribution from vehicular traffic (for both exhaust and non-exhaust emissions) was found to be slightly lower than in 2013–2014 ($1.6 \mu\text{g}/\text{m}^3$ in comparison with 2.1 – $2.3 \mu\text{g}/\text{m}^3$). The contribution of heavy oil combustion, on the contrary, was found to be elevated ($2.8 \mu\text{g}/\text{m}^3$ in the present study, versus $2.0 \mu\text{g}/\text{m}^3$ in 2014 and $0.8 \mu\text{g}/\text{m}^3$ in 2013). This source is considered to be related to shipping emissions, as well as industrial emissions from oil refineries located in the west of the Athens metropolitan area [54]. The increase in the heavy oil combustion contribution over the last years may be related to enhanced economic activities due to the gradual recovery of the Greek economy following the financial crisis.

The fourth anthropogenic source found in the present study was a mixed source of secondary aerosol formation and biomass burning. Previous studies have found separate sources related to secondary sulphates and nitrates and to biomass burning. The use of ionic species in some of these studies allowed for a better characterization of the impact of secondary aerosol formation on PM concentration levels [43,52]. In the present study, a secondary aerosol formation source with high loadings of S and organics was identified and may be associated with regional pollution [52]; however, it was not possible to identify locally produced secondary aerosol, which is usually traced by high loadings of nitrate [55].

Regarding the impact from biomass burning, as already discussed, the low OC/EC ratios measured during the cold period (average and median values equal to 5.0 and 4.5, respectively) and the low K levels suggest that biomass burning emissions during the study period were mainly related to the transport of wildfire smoke plumes, rather than local biomass burning for residential heating. According to the JRC Annual Fire Reports, Greece experienced increased levels of fire activity during the 2016 and 2017 fire seasons, which may have resulted in frequent transport events of aged biomass burning plumes, mixing with the regional pollution reaching the measurement site. The contribution of the mixed source (secondary aerosol formation and biomass burning) did not display significant temporal variability; specific peak contributions, though, may be associated with known wildfire events, such as the intense wildfires in Evia in August 2016 (at a distance of less than 100 km from the measurement site) (Figure S1, Supplementary Materials).

The inclusion of the hygroscopic growth factor (GF) in PMF analysis provided insight into the source apportionment of aerosol hygroscopicity, i.e., the contribution of the different particle sources to the total hygroscopicity of ambient aerosol. The mixed source related to secondary aerosol formation and biomass burning was found to be the most hydrophilic source, in agreement with previous source apportionment studies [31,32]. This source displayed high contributions by S and organics, as well as EC and K in lower loadings. Secondary inorganic aerosol, such as sulphate, is known to contribute significantly to atmospheric aerosol hygroscopicity [56]. In addition, highly oxidized secondary organic species have been found to play a major role in organic aerosol hygroscopicity [15,57]. On the other hand, the hygroscopic properties of biomass burning smoke plumes reported in the literature vary significantly, depending on biofuel characteristics, combustion conditions, plume's age (freshly emitted or aged plumes), and the presence of inorganic constituents [28]. Mochida and Kawamura [58] demonstrated that biomass burning emissions contain oxygenated organics that may significantly increase aerosol hygroscopicity. In addition, atmospheric ageing of biomass burning plumes is expected to lead to enhanced hygroscopic properties [9].

The hygroscopic growth rate was also associated with heavy oil combustion (24%) and vehicular exhaust emissions (19%). Li et al. have also found a small part of aerosol hygroscopicity associated with vehicular traffic and ship emissions [31]. The nearly hydrophobic particles emitted from fossil fuel combustion may be transformed into less-hygroscopic particles during atmospheric ageing processes, such as through condensation of secondary organic aerosols formed by photo-oxidation of volatile organic compounds emitted with exhaust gases [59,60]. The high S loading in the heavy oil combustion profile further promotes hygroscopicity.

Aged sea salt was also associated with hygroscopic growth (14%). Sea spray particles are inherently hygroscopic. Zieger et al. have demonstrated that the hygroscopic growth factor of sea salt particles is significantly lower than NaCl [61]. The presence of organics, also evident in the aged sea salt profile obtained by PMF, may further decrease the hygroscopicity of the ambient sea spray particles.

Vehicle non-exhaust emissions contributed very little to aerosol hygroscopicity, while mineral dust was the only source with no contribution to the hygroscopic GF, in agreement with Li et al. [31]. Given that major crustal components, such as Al- and Si-based compounds, are non-hygroscopic, mineral dust is generally considered insoluble and may suppress aerosol hygroscopicity [62,63].

The application of PMF analysis on combined chemical composition and hygroscopicity data may enhance our understanding of the hygroscopic properties of ambient aerosol in different types of environments, by identifying the various kinds of hygroscopic particles emitted by anthropogenic and natural sources or formed during atmospheric ageing. In addition, the inclusion in PMF analysis of OC carbon fractions (as provided by TOT method) may provide further insight with respect to the role of organics in aerosol hygroscopicity. The results of this study highlight the influence of the different source emissions and atmospheric ageing on the chemical composition and hygroscopic properties of atmospheric

aerosol. Good knowledge of the hygroscopic properties of ambient aerosol is important for air quality and visibility management, as well as climate research. Aerosol hygroscopicity has also been identified as a key parameter in terms of exposure to airborne particles and related health impacts. Taking into account that a large fraction of urban populations resides in suburban and urban background areas, understanding how the transformed emissions reaching the receptor site affect local aerosol hygroscopicity is crucial when developing mitigation measures for air quality and the protection of public health.

Supplementary Materials: The following supporting information can be downloaded at: <https://www.mdpi.com/article/10.3390/atmos13101685/s1>, Figure S1: Temporal variability of source contributions, obtained through the application of PMF model on PM_{2.5} chemical speciation data.

Author Contributions: E.D. and K.E. contributed to conceptualization and methodology; C.S., M.I.G., P.F., P.P., S.P., V.V. and E.D. contributed to data curation; P.F., P.P. and E.D. contributed to formal analysis, investigation, writing—original draft preparation, and visualization; all contributed to writing—review and editing; E.D. contributed to supervision; E.D., P.F., P.P. and M.I.G. contributed to funding acquisition. All authors have read and agreed to the published version of the manuscript.

Funding: This research is co-financed by Greece and the European Union (European Social Fund—ESF) through the Operational Programme «Human Resources Development, Education, and Lifelong Learning 2014–2020» in the context of the project “Study of the impact of emission sources and environmental conditions on the atmospheric aerosol mixture in the Athens Basin, with emphasis on particle hygroscopicity and related human health effects” (MIS 5047792).

Data Availability Statement: Data will be available by request to the authors.

Conflicts of Interest: The authors declare no conflict of interest. The funders had no role in the design of the study; in the collection, analyses, or interpretation of data; in the writing of the manuscript; or in the decision to publish the results.

References

1. Myhre, G.; Shindell, D.; Breon, F.-M.; Collins, W.; Fuglestedt, J.; Huang, J.; Koch, D.; Lamarque, J.-F.; Lee, D.S.; Mendoza, B.; et al. Anthropogenic and natural radiative forcing. In *Climate Change 2013: The Physical Science Basis, Contribution of Working Group I to the Fifth Assessment Report of the Intergovernmental Panel on Climate Change*; Stocker, T.F., Qin, D., Plattner, G.-K., Tignor, M.M.B., Allen, S.K., Boschung, J., Nauels, A., Xia, Y., Bex, V., Midgley, P.M., Eds.; Cambridge University Press: New York, NY, USA, 2013; pp. 659–740.
2. Beelen, R.; Hoek, G.; Raaschou-Nielsen, O.; Stafoggia, M.; Jovanovic Andersen, J.; Weinmayr, G.; Hoffmann, B.; Wolf, K.; Samoli, E.; Fischer, P.H.; et al. Natural-cause mortality and long-term exposure to particle components: An analysis of 19 European cohorts within the multi-center ESCAPE project. *Environ. Health Perspect.* **2015**, *123*, 525–533. [[CrossRef](#)]
3. Gasparini, R.; Li, R.; Collins, D.R. Integration of size distributions and size-resolved hygroscopicity measured during the Houston Supersite for compositional categorization of the aerosol. *Atmos. Environ.* **2004**, *38*, 3285–3303. [[CrossRef](#)]
4. Kerminen, V.-M. The effects of particle chemical character and atmospheric processes on particle hygroscopic properties. *J. Aerosol Sci.* **1997**, *28*, 121–132. [[CrossRef](#)]
5. Lai, L.W. Poor Visibility in Winter Due to Synergistic Effect Related to Fine Particulate Matter and Relative Humidity in the Taipei Metropolis, Taiwan. *Atmosphere* **2022**, *13*, 270. [[CrossRef](#)]
6. Massoli, P.; Bates, T.S.; Quinn, P.K.; Lack, D.A.; Baynard, T.; Lerner, B.M.; Tucker, S.C.; Brioude, J.; Stohl, A.; Williams, E.J. Aerosol optical and hygroscopic properties during TexAQS-GoMACCS 2006 and their impact on aerosol direct radiative forcing. *J. Geophys. Res. Atmos.* **2009**, *114*, D00F07. [[CrossRef](#)]
7. Malm, W.C.; Day, D.E. Estimates of aerosol species scattering characteristics as a function of relative humidity. *Atmos. Environ.* **2001**, *35*, 2845–2860. [[CrossRef](#)]
8. Väisänen, O.; Ruuskanen, A.; Ylisirniö, A.; Miettinen, P.; Portin, H.; Hao, L.; Leskinen, A.; Komppula, M.; Romakkaniemi, S.; Lehtinen, K.E.J.; et al. In-cloud measurements highlight the role of aerosol hygroscopicity in cloud droplet formation. *Atmos. Chem. Phys.* **2016**, *16*, 10385–10398. [[CrossRef](#)]
9. Vu, T.V.; Delgado-Saborit, J.M.; Harrison, R.M. A review of hygroscopic growth factors of submicron aerosols from different sources and its implication for calculation of lung deposition efficiency of ambient aerosols. *Air Qual. Atmos. Health* **2015**, *8*, 429–440. [[CrossRef](#)]
10. Broday, D.M.; Georgopoulos, P.G. Growth and deposition of hygroscopic particulate matter in the human lungs. *Aerosol Sci. Technol.* **2001**, *34*, 144–159. [[CrossRef](#)]
11. Krieger, U.K.; Marcolli, C.; Reid, J.P. Exploring the complexity of aerosol particle properties and processes using single particle techniques. *Chem. Soc. Rev.* **2012**, *41*, 6631–6662.

12. Choi, M.Y.; Chan, C.K. The effects of organic species on the hygroscopic behaviors of inorganic aerosols. *Environ. Sci. Technol.* **2002**, *36*, 2422–2428. [[CrossRef](#)] [[PubMed](#)]
13. Simoneit, B.R.T.; Rogge, W.F.; Mazurek, M.A.; Standley, L.J.; Cass, G.R. Lignan pyrolysis products, lignans, and renin acids as specified tracers of plant classes in emissions from biomass combustion. *Environ. Sci. Technol.* **1993**, *27*, 2533–2541. [[CrossRef](#)]
14. Jimenez, J.L.; Canagaratna, M.R.; Donahue, N.M.; Prevot, A.S.H.; Zhang, Q.; Kroll, J.H.; DeCarlo, P.F.; Allan, J.D.; Coe, H.; Ng, N.L.; et al. Evolution of organic aerosols in the atmosphere. *Science* **2009**, *326*, 1525–1529. [[CrossRef](#)] [[PubMed](#)]
15. Kuang, Y.; Huang, S.; Xue, B.; Luo, B.; Song, Q.; Chen, W.; Hu, W.; Li, W.; Zhao, P.; Cai, M.; et al. Contrasting effects of secondary organic aerosol formations on organic aerosol hygroscopicity. *Atmos. Chem. Phys.* **2021**, *21*, 10375–10391. [[CrossRef](#)]
16. Kanakidou, M.; Seinfeld, J.H.; Pandis, S.N.; Barnes, I.; Dentener, F.J.; Facchini, M.C.; Van Dingenen, R.; Ervens, B.; Nenes, A.; Nielsen, C.J.; et al. Organic aerosol and global climate modelling: A review. *Atmos. Chem. Phys.* **2005**, *5*, 1053–1123. [[CrossRef](#)]
17. Kong, L.; Hu, M.; Tan, Q.; Feng, M.; Qu, Y.; An, J.; Zhang, Y.; Liu, X.; Cheng, N. Aerosol optical properties under different pollution levels in the Pearl River Delta (PRD) region of China. *J. Environ. Sci.* **2020**, *87*, 49–59. [[CrossRef](#)]
18. Mandariya, A.K.; Tripathi, S.N.; Gupta, T.; Mishra, G. Wintertime hygroscopic growth factors (HGFs) of accumulation mode particles and their linkage to chemical composition in a heavily polluted urban atmosphere of Kanpur at the Centre of IGP, India: Impact of ambient relative humidity. *Sci. Total Environ.* **2020**, *704*, 135363. [[CrossRef](#)]
19. Wang, X.; Ye, X.; Chen, H.; Chen, J.; Yang, X.; Gross, D.S. Online hygroscopicity and chemical measurement of urban aerosol in Shanghai, China. *Atmos. Environ.* **2014**, *95*, 318–326. [[CrossRef](#)]
20. Liu, X.; Zhang, Y.; Jung, J.; Gu, J.; Li, Y.; Guo, S.; Chang, S.-Y.; Yue, D.; Lin, P.; Kim, Y.J.; et al. Research on the hygroscopic properties of aerosols by measurement and modeling during CAREBeijing-2006. *J. Geophys. Res.* **2009**, *114*, D00G16. [[CrossRef](#)]
21. Carrico, C.M.; Kreidenweis, S.M.; Malm, W.C.; Day, D.E.; Lee, T.; Carrillo, J.; McMeeking, G.R.; Collett, J.L., Jr. Hygroscopic growth behavior of a carbon-dominated aerosol in Yosemite National Park. *Atmos. Environ.* **2005**, *39*, 1393–1404. [[CrossRef](#)]
22. Stock, M.; Cheng, Y.F.; Birmili, W.; Massling, A.; Wehner, B.; Müller, T.; Leinert, S.; Kalivitis, N.; Mihalopoulos, N.; Wiedensohler, A. Hygroscopic properties of atmospheric aerosol particles over the Eastern Mediterranean: Implications for regional direct radiative forcing under clean and polluted conditions. *Atmos. Chem. Phys.* **2011**, *11*, 4251–4271. [[CrossRef](#)]
23. Gysel, M.; Crosier, J.; Topping, D.O.; Whitehead, J.D.; Bower, K.N.; Cubison, M.J.; Williams, P.I.; Flynn, M.J.; McFiggans, G.B.; Coe, H. Closure study between chemical composition and hygroscopic growth of aerosol particles during TORCH2. *Atmos. Chem. Phys.* **2007**, *7*, 6131–6144. [[CrossRef](#)]
24. Kreidenweis, S.M.; Remer, L.A.; Bruintjes, R.; Dubovik, O. Smoke aerosol from biomass burning in Mexico: Hygroscopic smoke optical model. *J. Geophys. Res.* **2001**, *106*, 4831–4844.
25. Grose, M.; Sakurai, H.; Savstrom, J.; Stolzenburg, M.R.; Watts, W.F.; Morgan, C.G.; Murray, I.P.; Twigg, M.V.; Kittelson, D.B.; McMurry, P.H. Chemical and physical properties of ultrafine diesel exhaust particles sampled downstream of a catalytic trap. *Environ. Sci. Technol.* **2006**, *40*, 5502–5507. [[CrossRef](#)] [[PubMed](#)]
26. Weingartner, E.; Burtscher, H.; Baltensperger, U. Hygroscopic properties of carbon and diesel soot particles. *Atmos. Environ.* **1997**, *31*, 2311–2327. [[CrossRef](#)]
27. Li, C.; Hu, Y.; Chen, J.; Ma, Z.; Ye, X.; Yang, X.; Wang, L.; Wang, X.; Mellouki, A. Physicochemical properties of carbonaceous aerosol from agricultural residue burning: Density, volatility, and hygroscopicity. *Atmos. Environ.* **2016**, *140*, 94–105. [[CrossRef](#)]
28. Carrico, C.M.; Petters, M.D.; Kreidenweis, S.M.; Sullivan, A.P.; McMeeking, G.R.; Levin, E.J.T.; Engling, G.; Malm, W.C.; Collett, J.L., Jr. Water uptake and chemical composition of fresh aerosols generated in open burning of biomass. *Atmos. Chem. Phys.* **2010**, *10*, 5165–5178. [[CrossRef](#)]
29. Lewis, K.A.; Arnott, W.P.; Moosmuller, H.; Chakrabarty, R.K.; Carrico, C.M.; Kreidenweis, S.M.; Day, D.E.; Malm, W.C.; Laskin, A.; Jimenez, J.L.; et al. Reduction in biomass burning aerosol light absorption upon humidification: Roles of inorganically-induced hygroscopicity, particle collapse, and photoacoustic heat and mass transfer. *Atmos. Chem. Phys.* **2009**, *9*, 8949–8966. [[CrossRef](#)]
30. Rissler, J.; Pagels, J.; Swietlicki, E.; Wierzbicka, A.; Strand, M.; Lillieblad, L.; Sanati, M.; Bohgard, M. Hygroscopic behaviour of aerosol particles emitted from biomass fired grate boilers. *Aerosol. Sci. Technol.* **2005**, *39*, 919–930. [[CrossRef](#)]
31. Li, J.; Zhang, Z.; Wu, Y.; Tao, J.; Xia, Y.; Wang, C.; Zhang, R. Effects of chemical compositions in fine particles and their identified sources on hygroscopic growth factor during dry season in urban Guangzhou of South China. *Sci. Total Environ.* **2021**, *801*, 149749. [[CrossRef](#)]
32. Vu, T.V.; Shi, Z.; Harrison, R.M. Estimation of hygroscopic growth properties of source-related sub-micrometre particle types in a mixed urban aerosol. *NPJ Clim. Atmos. Sci.* **2021**, *4*, 21. [[CrossRef](#)]
33. Bezantakos, S.; Barmounis, K.; Giamarelou, M.; Bossioli, E.; Tombrou, M.; Mihalopoulos, N.; Eleftheriadis, K.; Kalogiros, J.; Allan, J.D.; Bacak, A.; et al. Chemical composition and hygroscopic properties of aerosol particles over the Aegean Sea. *Atmos. Chem. Phys.* **2013**, *13*, 11595–11608. [[CrossRef](#)]
34. Petaja, T.; Kerminen, V.-M.; Dal Maso, M.; Junninen, H.; Koponen, I.K.; Hussein, T.; Aalto, P.P.; Andronopoulos, S.; Robin, D.; Hameri, K.; et al. Sub-micron atmospheric aerosols in the surroundings of Marseille and Athens: Physical characterization and new particle formation. *Atmos. Chem. Phys.* **2007**, *7*, 2705–2720. [[CrossRef](#)]
35. Spitieri, C.; Gini, M.; Gysel-Beer, M.; Eleftheriadis, K. Annual cycle of hygroscopic properties and mixing state of the suburban aerosol in Athens, Greece. *Atmos. Chem. Phys. Discuss.* **2022**. preprint. [[CrossRef](#)]
36. Eleftheriadis, K.; Gini, M.I.; Diapouli, E.; Vratolis, S.; Vasilatou, V.; Fetfatzis, P.; Manousakas, M.I. Aerosol microphysics and chemistry reveal the COVID19 lockdown impact on urban air quality. *Sci. Rep.* **2021**, *11*, 14477. [[CrossRef](#)] [[PubMed](#)]

37. Manousakas, M.; Diapouli, E.; Papaefthymiou, H.; Kantarelou, V.; Zarkadas, C.; Kalogridis, A.-C.; Karydas, A.-G.; Eleftheriadis, K. XRF characterization and source apportionment of PM₁₀ samples collected in a coastal city. *X Ray Spectrom.* **2018**, *47*, 190–200. [[CrossRef](#)]
38. Ma, J.; Li, X.; Gu, P.; Dallmann, T.R.; Presto, A.A.; Donahue, N.M. Estimating ambient particulate organic carbon concentrations and partitioning using thermal optical measurements and the volatility basis set. *Aerosol Sci. Technol.* **2016**, *50*, 638–651. [[CrossRef](#)]
39. Panteliadis, P.; Hafkenscheid, T.; Cary, B.; Diapouli, E.; Fischer, A.; Favez, O.; Quincey, P.; Viana, M.; Hitzenberger, R.; Vecchi, R.; et al. ECOC comparison exercise with identical thermal protocols after temperature offset correction-Instrument diagnostics by in-depth evaluation of operational parameters. *Atmos. Meas. Tech.* **2015**, *8*, 779–792. [[CrossRef](#)]
40. Belis, C.A.; Pernigotti, D.; Pirovano, G.; Favez, O.; Jaffrezo, J.L.; Kuenen, J.; van Der Gon, H.D.; Reizer, M.; Riffault, V.; Alleman, L.Y.; et al. Evaluation of receptor and chemical transport models for PM10 source apportionment. *Atmos. Environ. X* **2020**, *5*, 100053. [[CrossRef](#)]
41. Manousakas, M.; Papaefthymiou, H.; Diapouli, E.; Migliori, A.; Karydas, A.G.; Bogdanovic-Radovic, I.; Eleftheriadis, K. Assessment of PM_{2.5} sources and their corresponding level of uncertainty in a coastal urban area using EPA PMF 5.0 enhanced diagnostics. *Sci. Total Environ.* **2017**, *574*, 155–164. [[CrossRef](#)]
42. Pio, C.; Cerqueira, M.; Harrison, R.M.; Nunes, T.; Mirante, F.; Alves, C.; Oliveira, C.; Sanchez de la Campa, A.; Artíñano, B.; Matos, M. OC/EC ratio observations in Europe: Re-thinking the approach for apportionment between primary and secondary organic carbon. *Atmos. Environ.* **2011**, *45*, 6121–6132. [[CrossRef](#)]
43. Amato, F.; Alastuey, A.; Karanasiou, A.; Lucarelli, F.; Nava, S.; Calzolari, G.; Severi, M.; Becagli, S.; Gianelle, V.L.; Colombi, C.; et al. AIRUSE-LIFE+: A harmonized PM speciation and source apportionment in five southern European cities. *Atmos. Chem. Phys.* **2016**, *16*, 3289–3309. [[CrossRef](#)]
44. Li, H.Z.; Dallmann, T.R.; Li, X.; Gu, P.; Presto, A.A. Urban Organic Aerosol Exposure: Spatial Variations in Composition and Source Impacts. *Environ. Sci. Technol.* **2018**, *52*, 415–426. [[CrossRef](#)]
45. Kim, E.; Hopke, P.K. Source apportionment of fine particles in Washington, DC, utilizing temperature-resolved carbon fractions. *J. Air Waste Manag. Assoc.* **2004**, *54*, 773–785. [[CrossRef](#)] [[PubMed](#)]
46. Kim, E.; Hopke, P.K.; Edgerton, E.S. Improving source identification of Atlanta aerosol using temperature resolved carbon fractions in positive matrix factorization. *Atmos. Environ.* **2004**, *38*, 3349–3362. [[CrossRef](#)]
47. Jeong, H.; Ryu, J.-S.; Ra, K. Characteristics of potentially toxic elements and multi-isotope signatures (Cu, Zn, Pb) in non-exhaust traffic emission sources. *Environ. Pollut.* **2022**, *292*, 118339. [[CrossRef](#)]
48. Bove, M.C.; Brotto, P.; Cassola, F.; Cuccia, E.; Massabò, D.; Mazzino, A.; Piazzalunga, A.; Prati, P. An integrated PM_{2.5} source apportionment study: Positive Matrix Factorisation vs. the chemical transport model CAMx. *Atmos. Environ.* **2014**, *94*, 274–286. [[CrossRef](#)]
49. Pey, J.; Pérez, N.; Cortés, J.; Alastuey, A.; Querol, X. Chemical fingerprint and impact of shipping emissions over a western Mediterranean metropolis: Primary and aged contributions. *Sci. Total Environ.* **2013**, *463–464*, 497–507. [[CrossRef](#)]
50. Kim, E.; Hopke, P.K. Improving Source Apportionment of Fine Particles in the Eastern United States Utilizing Temperature-Resolved Carbon Fractions. *J. Air Waste Manag. Assoc.* **2005**, *55*, 1456–1463. [[CrossRef](#)]
51. Liu, W.; Wang, Y.; Russell, A.; Edgerton, E.S. Enhanced source identification of southeast aerosols using temperature-resolved carbon fractions and gas phase components. *Atmos. Environ.* **2006**, *40*, S445–S466. [[CrossRef](#)]
52. Diapouli, E.; Manousakas, M.; Vratolis, S.; Vasilatou, V.; Maggos, T.; Saraga, D.; Grigoratos, T.; Argyropoulos, G.; Voutsas, D.; Samara, C.; et al. Evolution of air pollution source contributions over one decade, derived by PM10 and PM2.5 source apportionment in two metropolitan urban areas in Greece. *Atmos. Environ.* **2017**, *164*, 416–430. [[CrossRef](#)]
53. Almeida, S.M.; Manousakas, M.; Diapouli, E.; Kertesz, Z.; Samek, L.; Hristova, E.; Sega, K.; Padilla Alvarez, R.; Belis, C.A.; The IAEA European Region Study GROUP. Ambient particulate matter source apportionment using receptor modelling in European and Central Asia urban areas. *Environ. Pollut.* **2020**, *266*, 115199. [[CrossRef](#)] [[PubMed](#)]
54. Karanasiou, A.A.; Siskos, P.A.; Eleftheriadis, K. Assessment of source apportionment by Positive Matrix Factorization analysis on fine and coarse urban aerosol size fractions. *Atmos. Environ.* **2009**, *43*, 3385–3395. [[CrossRef](#)]
55. Manousakas, M.; Diapouli, E.; Belis, C.; Vasilatou, V.; Gini, M.; Lucarelli, F.; Querol, X.; Eleftheriadis, K. Quantitative assessment of the variability in chemical profiles from source apportionment analysis of PM10 and PM2.5 at different sites within a large metropolitan area. *Environ. Res.* **2021**, *192*, 110257. [[CrossRef](#)]
56. Zieger, P.; Fierz-Schmidhauser, R.; Poulain, L.; Müller, T.; Birmili, W.; Spindler, G.; Wiedensohler, A.; Baltensperger, U.; Weingartner, E. Influence of water uptake on the aerosol particle light scattering coefficients of the central european aerosol. *Tellus Ser. B Chem. Phys. Meteorol.* **2014**, *66*, 22716. [[CrossRef](#)]
57. Duplissy, J.; DeCarlo, P.F.; Dommen, J.; Alfara, M.R.; Metzger, A.; Barmapadimos, I.; Prevot, A.S.H.; Weingartner, E.; Tritscher, T.; Gysel, M.; et al. Relating hygroscopicity and composition of organic aerosol particulate matter. *Atmos. Chem. Phys.* **2011**, *11*, 1155–1165. [[CrossRef](#)]
58. Mochida, M.; Kawamura, K. Hygroscopic properties of levoglucosan and related organic compounds characteristic to biomass burning aerosol particles. *J. Geophys. Res.* **2004**, *109*, D21202. [[CrossRef](#)]
59. Swietlicki, E.; Hansson, H.-C.; Hämeri, K.; Svenningsson, B.; Massling, A.; Mcfiggans, G.; McMurry, P.H.; Petäjä, T.; Tunved, P.; Gysel, M.; et al. Hygroscopic properties of submicrometer atmospheric aerosol particles measured with HTDMA instruments in various environments—A review. *Tellus B* **2008**, *60*, 432–469. [[CrossRef](#)]

60. Tritscher, T.; Jurányi, Z.; Martin, M.; Chirico, R.; Gysel, M.; Heringa, M.F.; DeCarlo, P.F.; Sierau, B.; Prévôt, A.S.H.; Weingartner, E.; et al. Changes of hygroscopicity and morphology during ageing of diesel soot. *Environ. Res. Lett.* **2011**, *6*, 034026. [[CrossRef](#)]
61. Zieger, P.; Vaisanen, O.; Corbin, J.C.; Partridge, D.G.; Bastelberger, S.; Mousavi-Fard, M.; Rosati, B.; Gysel, M.; Krieger, U.K.; Leck, C.; et al. Revising the hygroscopicity of inorganic sea salt particles. *Nat. Commun.* **2017**, *8*, 15883. [[CrossRef](#)]
62. Arub, Z.; Singh, G.; Habib, G.; Raman, R.S. Highly significant impact of mineral dust on aerosol hygroscopicity at New Delhi. *Atmos. Environ.* **2021**, *254*, 118375. [[CrossRef](#)]
63. Kelly, J.T.; Chuang, C.C.; Wexler, A.S. Influence of dust composition on cloud droplet formation. *Atmos. Environ.* **2007**, *41*, 2904–2916. [[CrossRef](#)]